Revised MS# ac-2016-05026f, 2/2017

Facile Colorimetric Detection of Silver Ions with Picomolar Sensitivity

Zhuangqiang Gao,[†,‡] Grace G. Liu,[§] Haihang Ye,[†] Robert Rauschendorfer,[†] Dianping Tang,[‡] and Xiaohu Xia[†,*]

[†]*Department of Chemistry, Michigan Technological University, Houghton, Michigan 49931, United States;*

[‡]*Key Laboratory of Analysis and Detection for Food Safety (Fujian Province & Ministry of Education), Collaborative Innovation Center of Detection Technology for Haixi Food Safety and Products (Fujian Province), Department of Chemistry, Fuzhou University, Fuzhou 350108, People's Republic of China;*

[§]*Houghton high school, Houghton, Michigan 49931, United States.*

*****To whom correspondence should be addressed. E-mail: xiaxh@mtu.edu (X. Xia)

Abstract

While various colorimetric methods have been actively developed for the detection of Ag^+ ions due to the simplicity and reliability, their limits of detection are confined to the level of nanomolar (nM). Here, we demonstrate a novel strategy for colorimetric Ag^+ detection with picomolar (pM) sensitivity. This strategy involves the use of polyvinylpyrrolidone (PVP)-capped Pt nanocubes as artificial peroxidases that can effectively generate color signal by catalyzing the oxidation of peroxidase substrates. In the presence of Ag^+ ions, the color signal generated from such Pt cubes would be greatly diminished because of the specific and efficient inhibition of Ag^+ toward the peroxidase-like activity of Pt cubes. This colorimetric method could achieve an ultralow detection limit of 80 pM and a wide dynamic range of 10^{-2}-10^4 nM. To the best of our knowledge, the method presented in this work showed the highest sensitivity for Ag^+ detection compared to all the reported colorimetric methods. Moreover, the method was also featured by simplicity and rapidness that was conducted at room temperature, in aqueous solution, and only took ~6 minutes.

Table of Contents

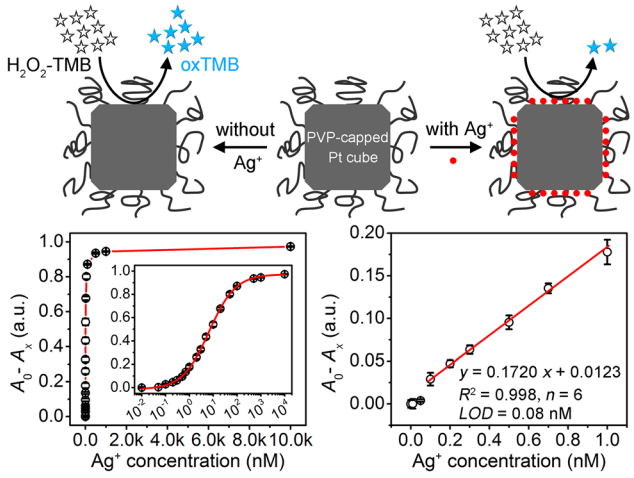

KEYWORDS: colorimetric detection; silver ions; platinum nanocubes; catalysis; sensitivity

INTRODUCTION

With the extensive use of metallic silver (Ag) and its compounds in industries and our daily life (*e.g.*, antimicrobial agents, catalysis, electronics, photography, and jewelry), Ag ions (Ag^+) contained wastewaters have been continuously discharged into the environment over the past several decades, especially in developing countries.[1-3] As one of the most hazardous heavy metal pollutants, Ag^+ ion is extremely toxic to humans at high doses.[1,2,4] In particular, Ag^+ ions can inactivate enzymes *via* binding to thiol, amino, and carboxyl groups and/or displacing other essential metal ions in functional enzymes, thereby seriously disrupting biological systems.[2,4] Based on the Secondary Drinking Water Standards from the United States Environmental Protection Agency (EPA), the maximum permissible level of Ag^+ ions in drinking water systems is 0.1 mg L^{-1} (or 0.93 μM). Accordingly, development of sensitive analytical methods for accurately detecting trace Ag^+ ions is of paramount importance for water quality control, public health, and environmental monitoring.

Typical sensitive techniques for Ag^+ ion detection include atomic absorption spectrometry (AAS), inductively coupled plasma-mass spectrometry or -optical emission spectrometry (ICP-MS or -OES), fluorescence spectroscopy, and voltammetry.[1,5] Nevertheless, these techniques generally require sophisticated instruments, complicated protocols, and skilled operators. Such requirements greatly limit practical applications of these techniques, especially in resource-limited areas such as remote villages. In contrast, colorimetric methods are broadly recognized as a kind of simple and cost-effective technique for Ag^+ detection because they can be easily performed by less-trained personnel with an inexpensive spectrophotometer or even naked eyes.[6-18] The most notable technique in colorimetric detection of Ag^+ ions is to utilize plasmonic Au or Ag nanoparticles because of its relatively high detection sensitivity.[9,12-14,16,18] Owing to the large extinction coefficients (which are several orders of magnitude higher than those of conventional organic dyes),[19,20] Au and Ag nanoparticles could display distinct color change through Ag^+-triggered interparticle distance or morphological alternations and thereby achieve relatively sensitive detection of Ag^+ ions. For instance, Tseng et al. modified the surface of

citrate-capped Au nanoparticles with Tween 20 as a stabilizer.[9] The reduction of Ag^+ ions by citrate ions led to the deposition of Ag on Au particle surfaces which displaced Tween 20. The displacement of Tween 20 triggered a red-to-blue color change of Au nanoparticles because the particles tended to aggregate without the stabilization by Tween 20. This colorimetric method could detect Ag^+ ions as low as 100 nM. Using the same Tween 20-stabilized Au nanoparticles, Chen et al. designed a reverse color change system (*i.e.*, blue-to-red) for Ag^+ detection by harnessing the ion redox-modulated surface chemistry, achieving a detection limit of 10 nM.[13] Similar to Tween-20, Ag^+-responsive C-base enriched single strand DNAs were also used to stabilize Au nanoparticles.[18] In the presence of Ag^+ ions, double strand structures of C-Ag^+-C base pairs were formed that compromised the stability of Au nanoparticles, leading to a red-to-blue color change. Despite of these demonstrations, the bottleneck for current colorimetric methods remains the low detection sensitivity (confined to the level of nM) relative to the aforementioned sophisticated instrument based techniques.

In this work, we demonstrate a novel strategy to break such confinement of low detection sensitivity for colorimetric Ag^+ detection. In this strategy, instead of relying on the plasmonic properties of Au or Ag nanoparticles, we take advantage of the excellent peroxidase-like activity of a unique type of Pt nanoparticles – polyvinylpyrrolidone-capped Pt nanocubes (PVP-capped Pt cubes[21]). Specifically, Ag^+ ions were found to be able to specifically and strongly bind to the surfaces of such PVP-capped Pt cubes, leading to the inhibition of peroxidase-like activity that could be easily monitored by a UV-vis spectrophotometer. This new strategy could push the detection limit of colorimetric method down to the regime of picomolar (pM), which is even lower than those of fluorescent methods (see Table S1 and associated discussions below for details). Significantly, the method was quite simple and rapid. The detection was conducted at room temperature in aqueous system and the entire procedure only took ~6 minutes. These distinctive features make this approach extremely suitable for on-site Ag^+ detection.

EXPERIMENTAL SECTIOIN

Materials and Reagents. Silver nitrate ($AgNO_3$, ≥99.0%), sodium hexachloroplatinate(IV) hexahydrate ($Na_2PtCl_6 \cdot 6H_2O$, 98%), potassium bromide (KBr, ≥99%), polyvinylpyrrolidone (PVP, M_W≈55,000), hydrogen peroxide solution (30 wt% in H_2O), 3,3',5,5'-tetramethylbenzidine (TMB, >99%), sodium acetate (NaOAc, ≥99%), acetic acid (HOAc, ≥99.7%), L-ascorbic acid (≥99%), gold(III) chloride trihydrate ($HAuCl_4 \cdot 3H_2O$, ≥99.9%), sodium nitrate ($NaNO_3$, ≥99%), silver trifluoroacetate (CF_3COOAg, ≥99.9%), sodium citrate dihydrate (≥99%), citric acid (≥99.5%), sodium borohydride ($NaBH_4$, ≥98%), and potassium chloride (KCl, ≥99%) were all obtained from Sigma-Aldrich. Ethylene glycol (EG) was obtained from J. T. Baker. All other reagents and chemicals were at least of analytical grade. All aqueous solutions were prepared using deionized (DI) water with a resistivity of 18.0 MΩ·cm. Tap water samples were collected from a household water pipe in our laboratory.

Synthesis of PVP-capped Pt Cubes. The PVP-capped Pt cubes were synthesized according to our recently reported procedure with minor modifications.[21] Briefly, in a standard synthesis, 3.5 mL of an EG solution containing 20 mg of KBr and 40 mg of PVP was hosted in a 20-mL vial and heated to 180 °C in an oil bath under magnetic stirring. Subsequently, 0.5 mL of $Na_2PtCl_6 \cdot 6H_2O$ solution (40 mg/mL, in EG) was added into the above solution with a pipette. The mixture was allowed to react for 20 min, and then was cooled down immediately with an ice-water bath. After being washed with acetone once and DI water twice *via* centrifugation, the final products (*i.e.*, PVP-capped Pt cubes) were stored in 4 mL of DI water for future use. The concentration of final products in terms of Pt element was determined to be 1.68 mg/mL by inductively coupled plasma-optical emission spectroscopy (ICP-OES). This Pt element concentration was converted to a Pt particle concentration of ~2.01×10^{14} particles/mL or ~3.34×10^{-7} M given that the shape and size of Pt particles (*i.e.*, cubes of 7.3 nm in edge length) had been resolved by transmission electron microscopy (TEM, see Figure 1B). PVP-capped Pt cubes with average edge lengths of 6.2 and 9.5 nm (shown in Figure S3) were obtained by using the same procedure for 7.3 nm Pt cubes except for the alternation of PVP amount from 40 mg to 8 and 200 mg PVP, respectively.

Standard Procedure for the Colorimetric Detection of Ag^+ Ions using PVP-capped Pt Cubes. Before detection, Ag^+ standards with various concentrations were prepared by using $AgNO_3$ as the source and 1.0 mM HOAc/NaOAc buffer (pH 6.0) as the sample matrix. Afterward, 590 μL of Ag^+ standards or samples was mixed with 10 μL of PVP-capped Pt cubes (~3.78×10^{10} particles/mL) in a disposable plastic cuvette, followed by incubation for 40 s at room temperature. Subsequently, 400 μL of substrate solution (5.0 M H_2O_2 and 2.0 mM TMB in 1.0 M HOAc/NaOAc buffer, pH 4.0) was added. After incubation for 5 min at room temperature, UV-vis spectrum and/or photograph of the reaction solutions were taken.

Synthesis of Other Nanostructures Shown in Figure 6. *i) 6.5 nm PVP-capped Pt spheres.* The 6.5 nm PVP-capped Pt spheres were synthesized using the same procedure as the 7.3 nm PVP-capped Pt cubes except for the exclusion of KBr in the reaction solution. The final products were stored in 4 mL of DI water at a particle concentration of ~5.38×10^{14} particles/mL or ~8.94×10^{-7} M; *ii) 5.0 nm citrate-capped Pt spheres.* The 5.0 nm citrate-capped Pt spheres were synthesized according to a previously reported procedure with minor modifications.[22] Briefly, 100 mL of 0.01% (w/v) $Na_2PtCl_6 \cdot 6H_2O$ aqueous solution was heated to boiling under vigorous stirring, followed by the addition of a 2 mL solution containing 1% sodium citrate and 0.05% citric acid. After 30 seconds, 1 mL of a freshly prepared solution containing 0.08% $NaBH_4$ and 1% sodium citrate was quickly added to the above solution. The resultant mixture was kept boiling and stirring for 10 min, and then cooled down to room temperature. The final products were stored in 10 mL of 0.1% sodium citrate solution at a particle concentration of ~2.21×10^{14} particles/mL or ~3.67×10^{-7} M; *iii) 5.9 nm PVP-capped Pd cubes.* The 5.9 nm PVP-capped Pd cubes were synthesized using our previously published procedure with slight changes.[23] In brief, 8.0 mL of an aqueous solution containing 105 mg of PVP, 60 mg of AA, 4 mg of KBr, and 186 mg of KCl was hosted in a vial and preheated to 80 °C in an oil bath under magnetic stirring for 10 min. Subsequently, 3.0 mL of an aqueous solution containing 57 mg of Na_2PdCl_4 was injected with a pipette. After the reaction had been proceeded for 3 h, the products were collected by centrifugation. The final PVP-capped Pd cubes were stored in 5.0 mL DI water at a particle concentration of ~1.56×10^{15}

particles/mL or ~2.59 × 10^{-6} M; *iv) 4.5 nm PVP-capped Au spheres*. 10.0 mL of an aqueous solution containing 1.05% (w/v) PVP and 0.25 mM $HAuCl_4$ was hosted in a vial and stirred at room temperature. Subsequently, 0.5 mL of a freshly prepared solution containing 0.08% $NaBH_4$ and 1% ascorbic acid was quickly added to the above solution. After the reaction had been proceeded for 10 min, the products were collected by centrifugation. The final PVP-capped Au spheres were stored in 5.0 mL DI water at a particle concentration of ~9.71 × 10^{13} particles/mL or ~1.61 × 10^{-7} M.

Characterizations. The UV-vis spectra were measured using an Agilent Cary 60 UV-vis spectrophotometer. TEM images were taken using a JEOL JEM-2010 microscope operated at 200 kV. The concentrations of Pt, Ag, and Pd ions were determined using an ICP-OES (Perkin Elmer Optima 7000DV), which could be converted into the particle concentrations of Pt and Pd nanoparticles by coupling with TEM imaging data. The X-ray photoelectron spectroscopy (XPS) measurements were performed on an SSX-100 system (Surface Science Laboratories, Inc.) equipped with a monochromated Al K_α X-ray source, a hemispherical sector analyzer (HSA), and a resistive anode detector. pH values of buffer solutions were recorded using an Oakton pH 700 benchtop meter. Photographs of samples in cuvettes were taken using a Canon EOS Rebel T5 digital camera.

RESULTS AND DISCUSSION

Detection Principle. As shown in Figure 1A, the detection relies on the high peroxidase-like catalytic activity of PVP-capped Pt cubes and the specific inhibition toward the catalytic activity by Ag^+ ions. We have recently demonstrated that the PVP-capped Pt cubes exhibit excellent peroxidase-like activity with an area specific catalytic efficiency (in terms of $K_{\text{cat-specific}}$, which is defined as the maximum number of reaction products generated per second per unit surface area of a catalyst[23]) as high as 2.5×10^3 $s^{-1}nm^{-2}$.[21] These cubes can efficiently catalyze the oxidation of 3,3',5,5'-tetramethylbenzidine (TMB, a typical peroxidase substrate[24,25]) by H_2O_2, generating intense blue color signal (*i.e.*, from oxidized TMB with a maximum absorbance at 653 nm[24]). In

the presence of Ag^+ ions, the surfaces of cubes are specifically and strongly passivated by Ag^+ through adsorption, thereby inhibiting the color signal generation process. The more Ag^+ ions in the system, the weaker color signal is generated from the catalytic reaction. As such, the concentration of Ag^+ ions could be conveniently determined by measuring the absorbance of the catalytic reaction solution using a UV-vis spectrometer. Alternatively, qualitative detection could be achieved with naked eyes.

Characterization of PVP-capped Pt cubes. Figure 1B shows a representative TEM image of the PVP-capped Pt cubes from a standard synthesis. Our analyses on 200 random particles indicated that ~80% of particles displayed well-defined cubic shapes, and the average edge length of the cubes was measured to be 7.3 nm with a narrow size distribution (0.6 nm in standard deviation). The high-resolution TEM image of an individual cube (inset in Figure 1B) clearly shows the corresponding lattice fringes and {100}-covered side faces. The lattice fringe spacing of 1.9 Å can be indexed to the {200} reflections of face-centered-cubic (*fcc*) Pt.[26] These TEM results demonstrated the successful preparation of PVP-capped Pt cubes with relatively high yield and good uniformity, which form the basis for the following design and experiments.

Demonstration of Detection Feasibility. We started with the feasibility demonstration of as-proposed colorimetric method for Ag^+ detection by involving Ag^+ ions into the PVP-capped Pt cubes catalyzed reaction (*i.e.*, oxidation of TMB by H_2O_2). As shown in Figure 1C, neither the PVP-capped Pt cubes as catalysts at a low concentration (*i.e.*, 3.78×10^{10} particles/mL, trace *a*) nor the TMB-H_2O_2 solution (trace *b*) showed distinguishable color. Only a mixture of them yielded blue-colored solution with a maximum absorbance at 653 nm ($A_{653\ nm} \approx 1.0$, trace *c*) that is the characteristic peak of oxidized TMB.[24,25] These observations confirmed the high peroxidase-like activity of the PVP-capped Pt cubes. Interestingly, when PVP-capped Pt cubes was incubated with colorless Ag^+ solution of 50 nM for 40 seconds prior to the mixture with TMB-H_2O_2 solution, the blue color intensity of the final reaction solution were greatly decreased ($A_{653\ nm} \approx 0.21$, trace *d*). Increase of the Ag^+ concentration further decreased the blue color intensity. At 10 μM Ag^+, the reaction solution was almost colorless ($A_{653\ nm} \approx 0.026$, trace *e*). These results implied that Ag^+ ions

could effectively inhibit the peroxidase-like activity of PVP-capped Pt cubes. To single out the role of Ag^+ ions, we conducted additional control experiments by replacing 50 nM $AgNO_3$ in trace *c* with 50 nM $NaNO_3$ and CF_3COOAg. As shown in Figure S1, the peroxidase-like activity of PVP-capped Pt cubes remained unchanged ($A_{653\ nm}$ = 0.99) after they had been treated with $NaNO_3$. In contrast, the activity of PVP-capped Pt cubes greatly decreased to an extent similar to what 50 nM $AgNO_3$ had caused ($A_{653\ nm}$ = 0.19) after they had been mixed with CF_3COOAg. These data verified that the inhibition of catalytic activity of Pt cubes was specifically attributed to Ag^+ ions. Taken together, this set of experiments demonstrated the feasibility of proposed colorimetric method for Ag^+ detection.

Sensitivity and Reproducibility. We then evaluated the detection sensitivity and reproducibility of the proposed colorimetric method. The detection was quite simple and straightforward. In a standard procedure, PVP-capped Pt cubes were incubated with Ag^+ standards or samples in a buffer solution held in a cuvette for a short period of time prior to mixing with TMB-H_2O_2 solution. After several minutes of reaction, the final reaction solution was subjected to readout by a UV-vis spectrometer, camera, or naked eyes (see Experimental Section for details). Based on the systematic examination of various experimental parameters (see Figure S2 for details), the optimal conditions for Ag^+ detection were found to be: *i*) room temperature (~22 °C) for the entire process; *ii*) pH 6.0 and incubation time of 40 s for the incubation of Ag^+ standards/samples with Pt cubes; *iii*) 0.8 mM TMB plus 2.0 M H_2O_2 for the TMB-H_2O_2 solution;[21,23] and *iv*) t = 5 min for the catalytic reaction. Taken together, the detection was conducted at room temperature and in aqueous solution, of which entire procedure only took ~6 minutes.

Figure 2A shows photographs of cuvettes containing final reaction solutions with Ag^+ standards ranging from 0 to 10,000 nM. It can be seen that the solutions displayed a continuous color change from deep blue to light blue and eventually to nearly colorless. Qualitative analysis with naked eyes could achieve a detection limit of ~5 nM Ag^+ ions. The detection results could be conveniently quantified with the aid of an ordinary UV-vis spectrometer. As shown in Figure 2B

and C, proportional decrease in absorbance at 653 nm of the reaction solutions associated with the concentration of Ag^+ ions were clearly seen. By plotting the decreased absorbance (A_0-A_x, where A_0 and A_x denote the absorbance at 653 nm for the blank and Ag^+ standard of x nM, respectively) against Ag^+ concentration, calibration curves for Ag^+ ions were generated (see Figure 2D, E). As indicated by Figure 2D, the color signal could be differentiated for Ag^+ ions in the range of 0.01-10,000 nM (6 orders of magnitudes), suggesting a wide response range of the colorimetric method toward Ag^+. As show by Figure 2E, a quality linear relationship (R^2 = 0.998) in the range of 0.1-1 nM Ag^+ could be observed. The limit of detection (LOD, defined as the concentration corresponding to a signal that is 3 times the standard deviation above the zero calibrator[27]) was calculated to be 80 pM. The coefficients of variation across the entire concentration range were between 0.13% and 7.64% (n = 6), indicating a good reproducibility of the method.

We also investigated the particle size effect on the detection performance. To this end, in addition to the 7.3 nm Pt cubes shown in Figure 1, we have prepared PVP-capped Pt cubes of two other sizes (*i.e.*, 6.2 and 9.5 nm, see Figure S3A and B) by simply varying the amount of PVP in a standard synthesis (see Experimental Section for details). As shown in Figure S3C, it was found that particle size in range of ~6.2-9.5 nm has no distinct impact on the detection performance.

To highlight the distinctive advantages of our method, we compared its analytical performance with those of previously reported methods for Ag^+ detection. As summarized in Table 1, our method exhibited a record-high detection sensitivity (LOD = 80 pM) among all the existing colorimetric methods. Significantly, it was even more sensitive than most fluorescent methods reported in literature (Table S1). In addition, the entire detection time of our method was only ~6 min, which was faster than most of the reported methods. Moreover, our method is cost-effective due to the usage of tiny amount of Pt cubes (~3×10^{-9} gram Pt per test) and ordinary reagents such as TMB and H_2O_2. The materials cost for each test was estimated to be less than 0.1 U.S. dollar.

The ultra-high detection sensitivity of our colorimetric method could be ascribed to the outstanding catalytic activity of the Pt cubes and the efficient inhibition of Ag^+ toward the catalysis

(will be discussed later), which together led to an amplified signal diminishment process. The magnitude of signal diminishment of the system could be quantified by comparing the amount of Ag^+ ions in the system with the amount of colored products diminished relative to the blank (*i.e.*, without Ag^+ ions). Taking the detection of 0.5 nM Ag^+ (in a volume of 590 μL) as an example, the presence of 2.95×10^{-13} mole Ag^+ ions corresponds to the diminishment of 2.45×10^{-9} mole oxidized TMB molecules (which was calculated based on their absorbance and molar absorption coefficient,[25] see Supporting Information for detailed calculation), suggesting an approximately 4-orders-of-magnitude signal amplification of the detection system.

Specificity Test. We also evaluated the specificity of our method toward other ionic species. Common cations (NH_4^+, Na^+, K^+, Li^+, Ba^{2+}, Ca^{2+}, Cd^{2+}, Co^{2+}, Cu^{2+}, Fe^{2+}, Mg^{2+}, Mn^{2+}, Ni^{2+}, Pb^{2+}, Zn^{2+}, Al^{3+}, Cr^{3+}, Fe^{3+}, Cu^+, Pd^{2+}, and Hg^{2+}) and anions (F^-, Cl^-, Br^-, NO_3^-, Ac^-, SO_3^{2-}, SO_4^{2-}, CO_3^{2-}, and PO_4^{3-}) as interfering ions were tested using the standard procedure. Note that Ag^+ was not involved in these interfering ions. Materials and procedures for preparing these interfering ions are provided in the Supporting Information. DI water and 5 nM of Ag^+ solution as the blank and control, respectively, were also tested. As shown in Figure 3, a significant decrease in absorbance at 653 nm relative to the blank was observed with Ag^+, while no distinct change in the absorbance was seen for all the interfering ions except for Pd^{2+} and Hg^{2+}. Nevertheless, the extents of decreased absorbance for Pd^{2+} and Hg^{2+} were much lower than that for Ag^+. These results indicated the relatively good specificity of the colorimetric method for detecting Ag^+ ions.

Demonstration of Real Sample Detection. To demonstrate the potential use of the proposed method in environmental scenarios, tap water samples (from the faucet of our laboratory) spiked with Ag^+ ions were analyzed. It should be mentioned that the original tap water was free of Ag^+ as confirmed by ICP-OES analysis. Specifically, 12 Ag^+-spiked tap water samples with Ag^+ concentrations at range of 0.4-100 nM were analyzed using the standard procedure. Ag^+ ions in each sample were quantified based on the calibration curve shown in Figure 2E. Note that samples with high Ag^+ concentration were diluted to load into the linear detection range (*i.e.*, 0.1-1 nM). The detection results were summarized in Figure 4 and Table 2. A strong positive correlation

between the spiked Ag^+ concentrations and the found Ag^+ concentrations was observed, with a slope of 0.9720 and an intercept of 0.0225, which were close to the ideal values of "1" and "0", respectively. The recoveries for all the samples were between 93.7% and 108.6%. The coefficients of variation for the quantification were in the range of 5.8%-12.6% (n = 3). These data demonstrated the capability of the proposed method for detection of Ag^+ ions in real-life samples.

Mechanistic Understanding. Finally, we designed and conducted a set of experiments with attempt to gain insights into the mechanism behind the detection. Because the peroxidase-like catalytic property of PVP-capped Pt cubes has been elaborated in our recent work,[21] the focus in this case was to understand how does Ag^+ inhibit the catalytic activity. We first performed XPS analysis to characterize the surfaces of PVP-capped Pt cubes before and after they had been incubated with Ag^+ ions. It should be noted that, after incubation with excess amount of Ag^+ ions, the Pt cubes were centrifuged and washed with DI water for ten times in order to remove free Ag^+ ions in the solution. Figure 5A shows the XPS survey spectra of the Pt cubes before and after Ag^+ incubation. The peaks for Pt 4f, C 1s, Pt 4d, N 1s, and O 1s at specific positions could be seen from the spectrum of initial Pt cubes, confirming the existence of PVP molecules on Pt cube surface.[28] For the cubes after incubation with Ag^+ ions, in addition to those characteristic peaks of PVP and Pt, peaks for Ag 3d were clearly observed,[29] indicating the adsorption of Ag^+ on the surface. Therefore, we assume that the binding of Ag^+ prevented TMB and/or H_2O_2 from accessing to Pt surfaces and thus inhibited the catalytic activity of the Pt cubes. It should be pointed out that the peak positions and relative intensities for PVP and Pt essentially remained unchanged after Ag^+ adsorption, implying that Ag^+ ions did not extensively react with or replace PVP molecules on the surface. Figure 5B and C show the high-resolution XPS spectra of the Pt 4f region for both Pt cube samples. No significant difference was observed for the two spectra, indicating a very weak chemical interaction between the adsorbed Ag^+ ions and Pt surface. Figure 5D shows the high-resolution XPS spectra of the Ag 3d region for the cubes after Ag^+ incubation, from which only Ag^+ peaks were resolved.[29] This observation indicated the existence of sole Ag(I) species on

the surface and further confirmed that almost no chemical reactions occurred between Ag^+ and PVP/Pt during the adsorption of Ag^+ ions.

To better understand the adsorption of Ag^+ ions on the PVP-capped Pt cubes, we conducted a comparison study by testing the efficiencies of Ag^+ ions in inhibiting the preoxidase-like activities of several other nanostructures of sub-10 nm in sizes. These nanostructures included 6.5 nm PVP-capped Pt nanospheres (Figure 6A), 5.0 nm citrate-capped Pt nanospheres (Figure 6B),[22] 5.9 nm PVP-capped Pd nanocubes (Figure 6C),[23] and 4.5 nm PVP-capped Au nanospheres (Figure 6D). The nanostructures were first incubated with Ag^+ ions and then utilized as catalysts for the oxidation of TMB by H_2O_2 using the standard procedure for PVP-capped Pt cubes, in which the ratio of Ag^+ ions to total surface area of each nanostructure was kept the same. The inhibition efficiency of Ag^+ toward catalytic activity was calculated based on $(A_0\text{-}A_x)/A_0$, where A_0 and A_x are the absorbances at 653 nm of the reaction solutions catalyzed by nanostructures before and after incubation with Ag^+ ions, respectively. Herein, the concentrations of nanostructures were set to certain values at which A_0 for all the nanostructures was normalized to ~1.0. Figure 6E compares the inhibition efficiencies of Ag^+ toward various nanostructures. It can be seen that the inhibition efficiency of Ag^+ toward PVP-capped Pt spheres was almost the same as that toward PVP-capped Pt cubes. This result indicated that Pt{100} facet of the Pt cubes was not the determinative factor in the adsorption of Ag^+ because the Pt spheres were encased by a combination of Pt{100} and Pt{111} facets.[30,31] In this regard, the performance of PVP-capped Pt spheres is expected to be as good as the PVP-capped Pt cubes in practical detection. In the present study, we focused on Pt cubes for demonstration mainly because they are more uniform in terms of both shape and size relative to Pt spheres, which makes it convenient to gain quantitative understanding on the detection mechanism. In contrast, the inhibition efficiency toward citrate-capped Pt spheres was much lower compared to the PVP-capped Pt cubes or spheres (see Figure 6E), suggesting that PVP played an important role in faciliating the adsorption of Ag^+ ions.[32-35] Based on these results, we hypothesize that the strong adsorption of Ag^+ ions on PVP-capped Pt cubes was ascribed to the synergistic effect of the *fcc* crystal structure of Pt and PVP. In particular, a good match in geometry

between Ag^+ and the *fcc* structure of Pt might promote the Ag^+ adsorption.[36] This argument was supported by the facts that: *i*) similar inhibition efficiency of Ag^+ was observed for PVP-capped cubes made of Pd (Figure 6E), of which lattice constance is almost the same as that of Pt (<1% in lattice mismatch[37,38]); and *ii*) Ag^+ could not inhibit the peroxidase-like activity of PVP-capped Au nanospheres (Figure 6E). Note that the lattice mismatch between Pt and Au is as large as 3.8%.[39] In addition, such argument was, to some extent, also supported by the data shown in Figure 3. In particular, Hg^{2+} could also inhibit the peroxidase-like activity of PVP-capped Pt cubes even though its inhibition efficiency was lower than that of Ag^+. This observation might be ascribed to the fact that the ionic radius of Hg^{2+} is similar to that of Ag^+ (0.126 nm *vs.* 0.110 nm),[40,41] which ensures a relatively good match between Hg^{2+} and the Pt *fcc* structure. To further demonstrate this synergistic effect, we carried out another control experiment, in which the same amount of Ag^+ ions were pre-incubated with excess PVP and then applied to inhibit the catalytic activity of PVP-capped Pt cubes (Figure 6F). Interestingly, the inhibition efficiency of Ag^+ was almost the same as that of the case without the pre-incubation with free PVP. This result suggested that free PVP barely bound to Ag^+ ions, and only the combination of PVP and Pt surface could induce the strong adsorption of Ag^+ ions.

To gain quantitative analysis, we determined the coverage density of Ag^+ on PVP-capped Pt cubes by using ICP-OES. The cubes were first incubated with excess amount of Ag^+ ions and washed ten times with DI water *via* centrifuge. The resultant Ag^+ adsorbed Pt cubes were digested with aqua regia and then subjected to ICP-OES analysis. The molar ratio of Ag to Pt element was quantified to be 0.074:1. Based on this data, the size of Pt cubes, and the unit cell parameters of Ag,[42,43] the average number of Ag atomic layers adsorbed on the Pt cubes was estimated to be 0.972. This result suggested the nearly monolayer adsorption of Ag^+ ions on Pt cube surface. This result further demonstrated that Ag^+ ions absorbed at the interface between Pt and PVP rather than the repeating units of polymeric PVP molecules. In a sense, the unique interface of Pt and PVP was specific to Ag^+ binding. Taken together, the synergistic adsorption effect of the Pt *fcc* crystal structure and PVP was believed to be responsible for the specific and strong adsorption of Ag ions

on the surface of PVP-capped Pt cubes. This adsorption of Ag^+ blocked the active sites for catalysis and eventually inhibited the peroxidase-like catalytic activity of the Pt cubes.

CONCLUSIONS

In summary, we have demonstrated a facile colorimetric method for the detection of Ag^+ ions with picomolar sensitivity. The high detection sensitivity relies on the ultrahigh peroxidase-like catalytic activity of PVP-capped Pt cubes and the specific, efficient inhibition toward the catalytic activity by Ag^+ ions. In addition to the high sensitivity, the colorimetric method was also featured by simple operation, rapidness, and cost effectiveness. We believe the method presented here will find widespread use in monitoring and quantifying Ag^+ ions in environmental senariors. The concept on taking advantage of the superior catalytic activities of nanoscale artificial peroxidases may be extended to the detection and sensing of other critical ionic species.[44,45]

ASSOCIATED CONTENT

Supporting Information

Additional information, tables, figures, and methods for calculations. The Supporting Information is available free of charge on the ACS Publications website at DOI: 10.1021/acs.analchem.00.

AUTHOR INFORMATION

Corresponding Author

*E-mail: xiaxh@mtu.edu (X. Xia)

Notes

The authors declare no competing financial interest.

ACKNOWLEDGMENTS

This work was supported by the National Science Foundation (NSF) Career Award (CHE-1651307), the Michigan Translational Research & Commercialization Fund (MTRAC), Grant Case-48161 of the 21st Century Jobs Trust Fund received through the Michigan Strategic Fund from the State of Michigan, and the startup funds from Michigan Technological University. The MTRAC program is funded by the Michigan Strategic Fund with program oversight by the Michigan Economic Development Corporation. We thank Dr. Yuzi Liu from the Center for Nanoscale Materials at Argonne National Laboratory for assistance with TEM imaging.

REFERENCE

(1) Howe, P. D.; Dobson, S.; World Health Organization. *Silver and Silver Compounds*; World Health Organization: Geneva, **2002**.

(2) Drake, P. L.; Hazelwood, K. J. *Ann. Occup. Hyg.* **2005**, *49*, 575-585.

(3) Saran, R.; Liu, J. *Anal. Chem.* **2016**, *88*, 4014-4020.

(4) Ratte, H. T. *Environ. Toxicol. Chem.* **1999**, *18*, 89-108.

(5) Barriada, J. L.; Tappin, A. D.; Evans, E. H.; Achterberg, E. P. *Trends Anal. Chem.* **2007**, *26*, 809-817.

(6) Song, Y.; Wei, W.; Qu, X. *Adv. Mater.* **2011**, *23*, 4215-4236

(7) Gao, Z.; Deng, K.; Wang, X.; Miró, M.; Tang, D. *ACS Appl. Mater. Interfaces* **2014**, *6*, 18243-18250.

(8) Chang, Y.; Zhang, Z.; Hao, J.; Yang, W.; Tang, J. *Sens. Actuators, B* **2016**, *232*, 692-697.

(9) Lin, C.; Yu, C.; Lin, Y.; Tseng, W. *Anal. Chem.* **2010**, *82*, 6830-6837.

(10) Zhou, X.; Kong, D.; Shen, H. *Anal. Chem.* **2010**, *82*, 789-793.

(11) Liu, S.; Tian, J.; Wang, L.; Sun, X. *Sens. Actuators, B* **2012**, *165*, 44-47.

(12) Huang, H.; Qu, C.; Liu, X.; Huang, S.; Xu, Z.; Liao, B.; Zeng, Y.; Chu, P. K. *ACS Appl. Mater. Interfaces* **2011**, *3*, 183-190.

(13) Luo, T.; Chen, Z.; Wang, Y.; Chen, L. *ACS Appl. Mater. Interfaces* **2011**, *3*, 1568-1573.

(14) Liu, Y.; Dai, J.; Xu, L.; Liu, X.; Liu, J.; Li, G. *Sens. Actuators, B* **2016**, *237*, 216-223.

(15) Zhou, X.; Kong, D.; Shen, H. *Anal. Chim. Acta* **2010**, *678*, 124-127.

(16) Sung, Y.; Wu, S. *Sens. Actuators, B* **2014**, *197*, 172-176.

(17) Li, T.; Shi, L.; Wang, E.; Dong, S. *Chem. Eur. J.* **2009**, *15*, 3347-3350.

(18) Li, B.; Du, Y.; Dong, S. *Anal. Chim. Acta* **2009**, *644*, 78-82.

(19) Rycenga M.; Cobley, C. M.; Zeng, J.; Li, W.; Moran, C. H.; Zhang, Q.; Qin, D.; Xia, Y. *Chem. Rev.* **2011**, *111*, 3669-3712.

(20) Jain, P. K.; Lee, K. S.; El-Sayed, I. H.; El-Sayed, M. A. *J. Phys. Chem. B* **2006**, *110*, 7238-7248.

(21) Ye, H.; Liu, Y.; Chhabra, A.; Lilla, E.; Xia, X. *ChemNanoMat* **2017**, *3*, 33-38.

(22) Bigall, N. C.; Halrtling, T.; Klose, M.; Simon, P.; Eng, L. M.; Eychmuller, A. *Nano Lett.* **2008**, *8*, 4588-4592.

(23) Xia, X.; Zhang, J.; Lu, N.; Kim, M. J.; Ghale, K.; Xu, Y.; McKenzie, E.; Liu, J.; Ye, H. *ACS Nano* **2015**, *9*, 9994-10004.

(24) Josephy, P. D.; Eling, T. E.; Mason, R. P. *J. Biol. Chem.* **1982**, *257*, 3669-3675.

(25) Gao, L.; Zhuang, J.; Nie, L.; Zhang, J.; Zhang, Y.; Gu, N.; Wang, T.; Feng, J.; Yang, D.; Perrett, S.; et al. *Nat. Nanotechnol.* **2007**, *2*, 577-583.

(26) Wang, C.; Daimon, H.; Lee, Y.; Kim, J.; Sun, S. *J. Am. Chem. Soc.* **2007**, *129*, 6974-6975.

(27) Armbruster, D. A.; Tillman, M. D.; Hubbs, L. M. *Clin. Chem.* **1994**, *40*, 1233-1238.

(28) Aliaga, C.; Park, J. Y.; Yamada, Y.; Lee, H. S.; Tsung, C.-K.; Yang, P.; Somorjai, G. A. *J. Phys. Chem. C* **2009**, *113*, 6150-6155.

(29) Yin, L.; Wang, Z.; Lu, L.; Wan, X.; Shi, H. *New J. Chem.* **2015**, *39*, 4891-4900.

(30) Xia, Y.; Xia, X.; Peng, H.-C. *J. Am. Chem. Soc.* **2015**, *137*, 7947-7966.

(31) Xia, Y.; Jiong, Y.; Lim, B.; Skrabalak, S. E. *Angew. Chem., Int. Ed.* **2009**, *48*, 60-103.

(32) Pastoriza-Santos, I.; Liz-Marzán, L. M. *Langmuir* **2002**, 18, 2888-2894.

(33) Koczkur, K. M.; Mourdikoudis, S.; Polavarapu, L.; Skrabalak, S. E. *Dalton Trans.* **2015**, *44*, 17883-17905.

(34) Silvert, P.-Y.; Herrera-Urbina, R.; Duvauchelle, N.; Vijayakrishnan, V.; Elhsissen, K. T. *J. Mater. Chem.* **1996**, *6*, 573-577.

(35)Huang, H. H.; Ni, X. P.; Loy, G. L.; Chew, C. H.; Tan, K. L.; Loh, F. C.; Deng, J. F.; Xu, G. Q. *Langmuir* **1996,** *12,* 909-912.

(36) Xia, X.; Zeng, J.; Zhang, Q.; Moran, C. H.; Xia, Y. *J. Phys. Chem. C* **2012**, *116*, 21647-21656.

(37) Habas, S. E.; Lee, H.; Radmilovic, V.; Somorjai, G. A.; Yang, P. *Nat. Mater.* **2007**, *6*, 692-697.

(38) Zhang, Y.; Bu, L.; Jiang, K.; Guo, S.; Huang, X. *Small* **2016**, *12*, 706-712.

(39) Feng, L.; Wu, X.; Ren, L.; Xiang, Y.; He, W.; Zhang, K.; Zhou, Y.; Xie, S. *Chem.-Eur. J.* **2008**, *14*, 9764-9771.

(40) Tan, G.; Shi, F.; Doak, J. W.; Sun, H.; Zhao, L.; Wang, P.; Uher, C.; Wolverton, C.; Dravid, V. P.; Kanatzidis, M. G. *Energy Environ. Sci.* **2015**, *8*, 267-277.

(41) Huang, S.; Wen, Z.; Zhu, X.; Gu, Z. *Electrochem. Commun.* **2004**, *6*, 1093-1097.

(42) Yang, Y.; Liu, J.; Fu, Z.; Qin, D. *J. Am. Chem. Soc.* **2014**, *136*, 8153-8156.

(43) Cathcart, N.; Coombs, N.; Gourevich, I.; Kitaev, V. *Nanoscale* **2016**, *8*, 18282-18290.

(44) Wu, G.-W.; He, S.-B.; Peng, H.-P.; Deng, H.-H.; Liu, A.-L.; Lin, X.-H.; Xia, X.-H.; Chen, W. *Anal. Chem.* **2014**, *86*, 10955-10960.

(45) Li, W.; Chen, B.; Zhang, H.; Sun, Y.; Wang, J.; Zhang, J.; Fu, Y. *Biosens. Bioelectron.* **2015**, *66*, 251-258.

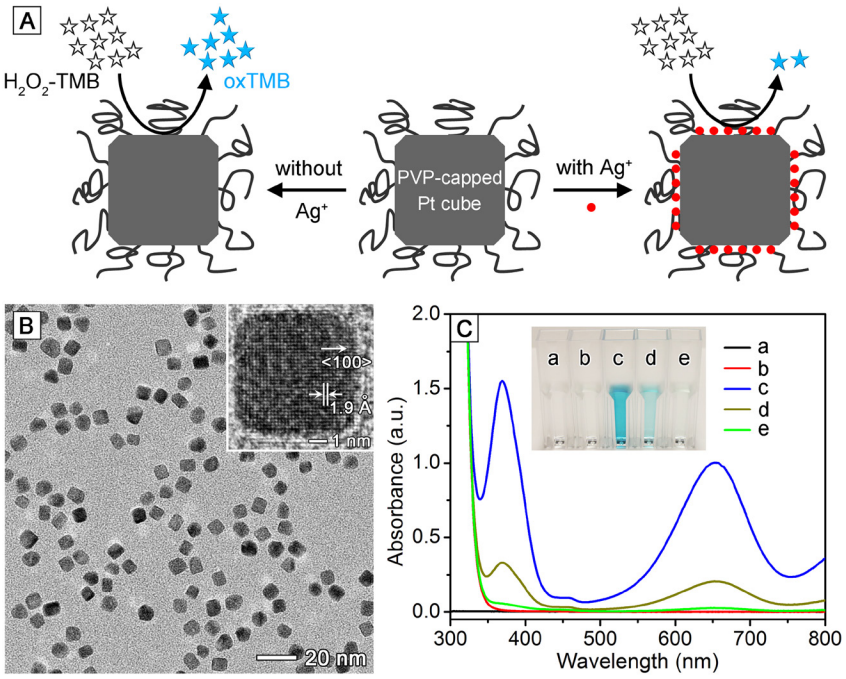

Figure 1. PVP-capped Pt cubes for colorimetric detection of Ag^+ ions. (A) Schematics of detection principle; (B) TEM image of the PVP-capped Pt cubes. Inset shows the HRTEM image of an individual Pt cube; (C) Photographs and corresponding UV-vis spectra taken from solutions in cuvettes containing: a) PVP-capped Pt cubes (~3.78×10^{10} particles/mL), b) TMB-H_2O_2, c) PVP-capped Pt cubes + (TMB-H_2O_2), d) 50 nM $AgNO_3$ + PVP-capped Pt cubes + (TMB-H_2O_2), and e) 10 μM $AgNO_3$ + PVP-capped Pt cubes + (TMB-H_2O_2).

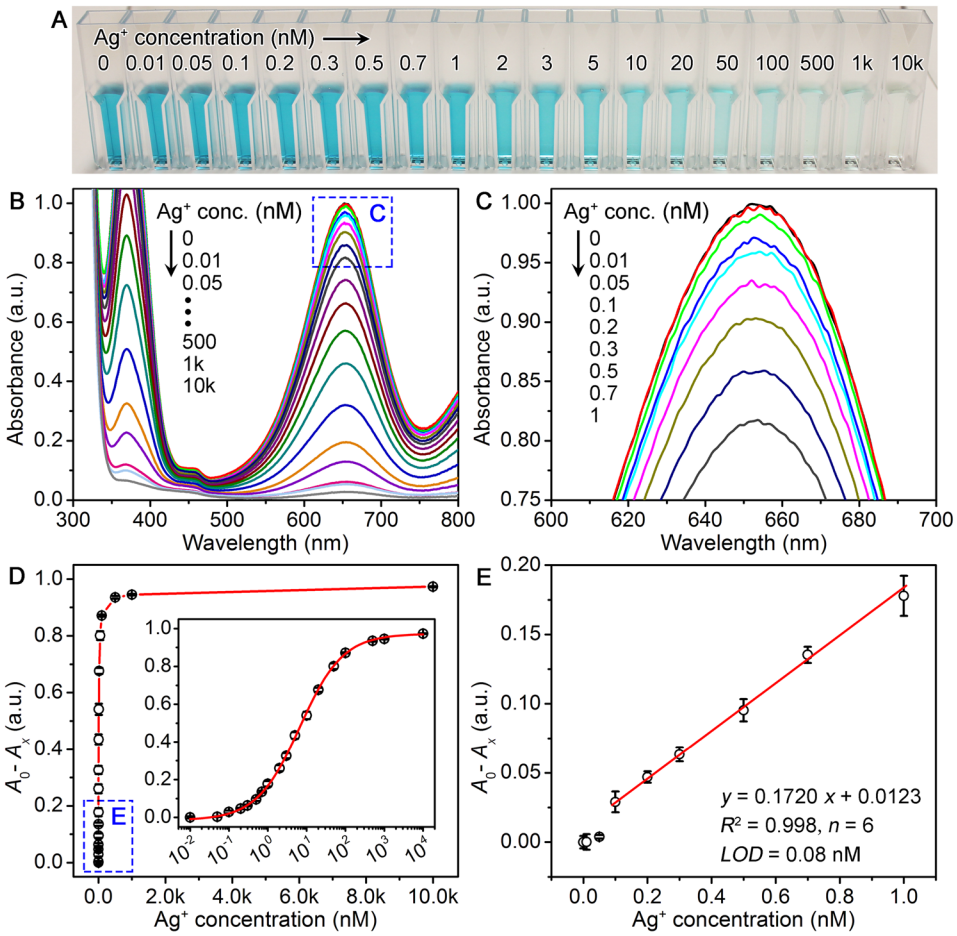

Figure 2. Detection of Ag^+ standards using the PVP-capped Pt cubes based colorimetric method. (A) Photographs showing the final reaction solutions with different Ag^+ standards in cuvettes; (B) Corresponding UV-vis spectra taken from the samples shown in (A); (C) Magnified UV-vis spectra of the region marked by a blue box in (B); (D) Calibration curve generated by plotting the decrease of the absorbance at 653 nm relative to the blank for reaction solutions (A_0-A_x) as a function of the Ag^+ concentration. Inset shows the same plot on a logarithmic scale; (E) Linear region of the calibration curve shown in (D). In (D) and (E), error bar represents the standard deviation of six independent measurements (n = 6).

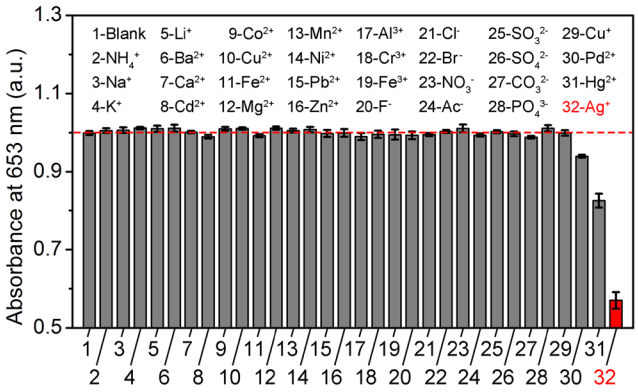

Figure 3. Specificity test of the developed colorimetric method. Intensities of the absorbance at 653 nm were recorded from the reaction solutions that were conducted with various ionic species using the standard procedure for Ag^+ detection. The numbers under each bar correspond to the ions marked with the same numbers. Blank (#1) denotes DI water. The ionic concentrations for samples #2-#28 and samples #29-#32 were 50 nM and 5 nM, respectively. Error bar represents the standard deviation of three independent measurements (n = 3). Chemicals and procedures for the preparation of all ionic solutions are provided in the Supporting Information.

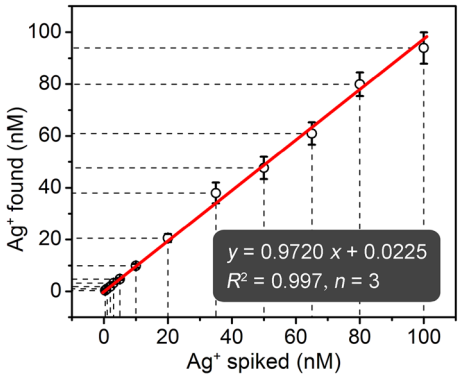

Figure 4. Correlation analysis between Ag^+ concentrations in 12 Ag^+-spiked tap water samples and the Ag^+ concentrations found by the developed colorimetric method. Error bar represents the standard deviation of three independent measurements (n = 3). Quantitative data and recovery of each sample were summarized in Table 2.

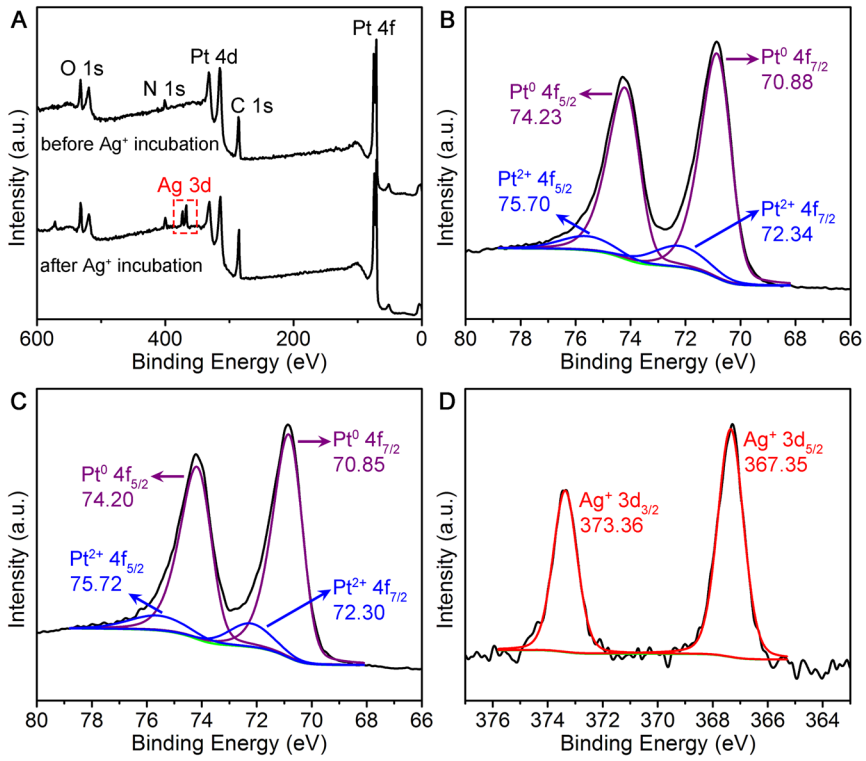

Figure 5. XPS analyses of the PVP-capped Pt cubes before and after incubation with Ag^+ ions. (A) XPS survey spectra of both samples; (B, C) Pt 4f XPS spectra of the Pt cubes before (B) and after (C) incubation with Ag^+; (D) Ag 3d XPS spectrum of the Pt cubes after incubation with Ag^+ ions.

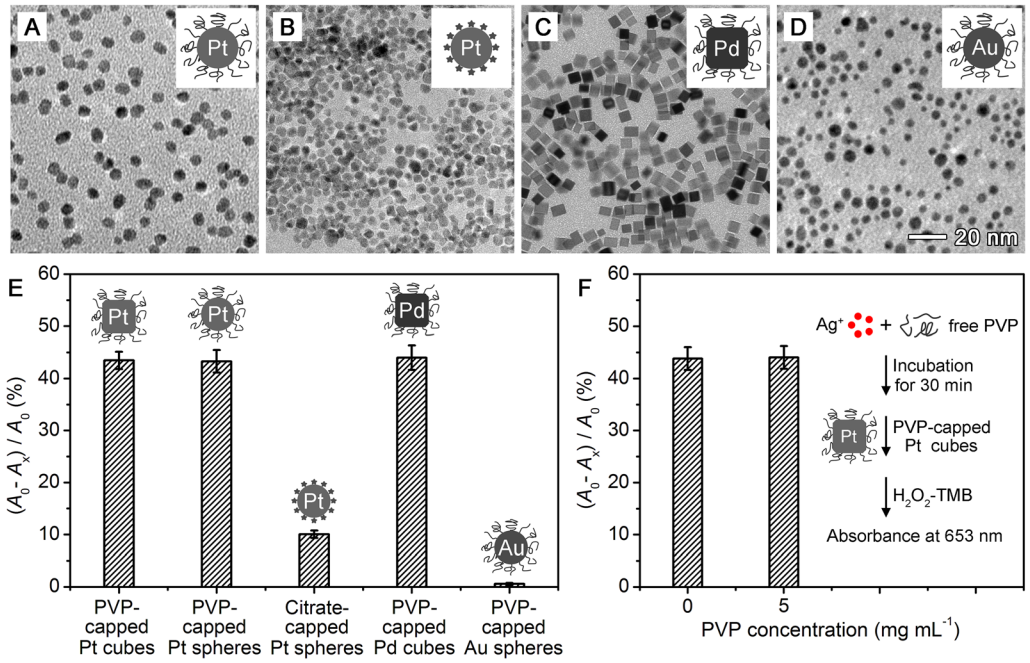

Figure 6. The inhibition of Ag^+ toward the peroxidase-like activities of various nanostructures. (A-D) TEM images of: (A) 6.5 nm PVP-capped Pt spheres, (B) 5.0 nm citrate-capped Pt spheres, (C) 5.9 nm PVP-capped Pd cubes, and (D) 4.5 nm PVP-capped Au spheres; (E) Inhibition efficiencies of Ag^+ toward the peroxidase-like activities of different nanostructures. (F) Inhibition efficiencies of Ag^+ toward the peroxidase-like activities of two PVP-capped Pt cube samples (from the same batch of synthesis) that were pre-incubated with 0 and 5 mg/mL PVP aqueous solution, respectively. In (E) and (F), A_0 and A_x are the absorbances at 653 nm of reaction solutions catalyzed by certain nanostructures before and after incubation with Ag^+ ions, respectively. The concentrations of nanostructures were set to certain values at which A_0 for all the nanostructures was normalized to ~1.0. Error bar represents the standard deviation of three independent measurements (n = 3).

Table 1. Comparison of analytical performances of various colorimetric methods for Ag^+ detection. LOD = limit of detection.

Method	Detection probes	LOD (nM)	Assay time (min)	Refs
Colorimetric methods	BSA -stabilized Au clusters	204	10	8
	Tween 20-Au nanoparticles	100	5	9
	G-quadruplex-hemin DNAzyme	64	110	10
	3,3′,5,5′,-tetramethylbenzidine	50	30	11
	Core-shell Au nanoparticles	10	15	12
	Tween 20-Au nanoparticles	10	33	13
	Au-Ag core-shell nanoparticles	8.76	4	14
	G-quadruplex-hemin DNAzyme	6.3	110	15
	N-1-(2-mercaptoethyl)adenine -Au nanoparticles	3.3	20	16
	DNAzyme switch	2.5	4	17
	DNA-Au nanoparticles	0.59	32	18
	PVP-capped Pt cubes	0.08	6	This work

Table 2. Summary of the detection of Ag^+ from spiked tap water samples as shown in Figure 4. Recovery is defined as the found amount of Ag^+ ions divided by the Ag^+ ions originally spiked in a sample. SD = standard deviation (n = 3), CV = coefficient of variation.

Sample no.	Spiked (nM)	Found (mean ± SD) (nM)	CV (%)	Recovery (%)
1	0.4	0.41 ± 0.04	9.8	104.1
2	1	1.03 ± 0.13	12.6	103.4
3	2	1.91 ± 0.12	6.3	95.5
4	3	3.26 ± 0.32	9.8	108.6
5	5	4.80 ± 0.39	8.1	95.9
6	10	9.86 ± 0.71	7.2	98.6
7	20	20.6 ± 1.5	7.3	102.8
8	35	38.0 ± 4.0	10.5	108.4
9	50	47.6 ± 4.3	9.0	95.2
10	65	60.9 ± 4.3	7.1	93.7
11	80	79.9 ± 4.6	5.8	99.9
12	100	93.9 ± 6.0	6.4	93.9